

## CRACK EXTENSION AND KINKING IN LAMINATES AND BICRYSTALS

TZU-CHIANG WANG† and C. FONG SHIH

Division of Engineering, Brown University, Providence, RI 02912, U.S.A.

and

ZHIGANG SUO

Department of Mechanical Engineering, University of California, Santa Barbara, CA 93106,  
U.S.A.

(Received 22 August 1990)

**Abstract**—Singular fields at the tip of an interface crack in anisotropic solids are reviewed with emphasis on establishing a framework to quantify fracture resistance under mixed mode conditions. The concepts of mode mixity and surface toughness are unified by using generalized interface traction components. The similarity between the anisotropic theory and existing isotropic theory is shown. Explicit formulae are given for misoriented orthotropic bimetals with potential applications envisioned including composite laminates and semiconductor crystals. Competition between crack extension along the interface and kinking into the substrate is investigated using a boundary layer formulation. Several case studies reveal the role of anisotropy. An explicit complex variable representation for orthotropic materials and a solution to a dislocation interacting with a crack are presented in two self-contained Appendices.

### 1. INTRODUCTION

Substantial progress has been made on the mechanics of interface fracture. The recent development is assessed in an *Acta Scripta Metallurgica Proceeding* edited by Ruhle *et al.* (1990). An engineering program has emerged which allows the fracture resistance of interfaces to be measured and utilized. Specimen geometries suitable for fracture testing are rigorously calibrated (Suo and Hutchinson, 1989; Charalambides *et al.*, 1989; O'Dowd *et al.*, 1991). The program has been implemented in experiments by several groups (Cao and Evans, 1989; Wang and Suo, 1990; Liechti and Chai, 1991). Applications are made to thin films, adhesive joints, and composite laminates (see Hutchinson and Suo, 1991).

An empirical fact is that the fracture resistance of an interface depends strongly on the *mode mixity*, the relative proportion of the opening and sliding tractions ahead of the crack tip. The concepts of mode mixity and surface toughness have recently been rationalized by Rice (1988) for interfaces in isotropic solids on the basis of small-scale irregularities (contact zone, inelastic zone, etc.). These concepts are extended here by applying several unifying results due to Suo (1990) to solids of arbitrary anisotropy. The mode mixities will be defined by the generalized interface traction components ahead of the crack tip. Explicit results, listed for misoriented orthotropic solids, lend themselves to immediate applications to cross-ply laminates and brittle bicrystals. Experimental aspects of determining surface toughnesses are briefly discussed.

A complexity in interfacial fracture testing is that, under mixed mode load, the crack has a strong tendency to kink into the substrate. Crack kinking has been observed for brittle substrates as glasses, ceramics and polymers. Semiconductor crystals provide another example where the crack may kink onto preferred crystallographic planes. The question of whether the crack will extend along the interface, or kink into the substrate is addressed in

† Permanent address: Institute of Mechanics, Chinese Academy of Sciences, Beijing, China.

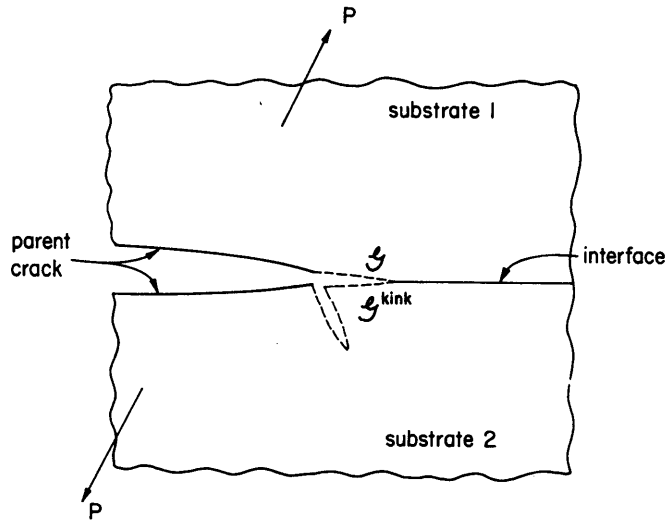


Fig. 1. A bimaterial interface crack subject to mixed mode loading. Two virtual crack directions and their driving forces are indicated.

this paper. Figure 1 illustrates the two competing virtual crack extension directions, where  $\mathcal{G}$  and  $\mathcal{G}^{\text{kink}}$  are the energy release rates for the crack to extend along, and kink out of, the interface. These crack driving forces depend on the magnitude of the applied loads, the relative proportion of the opening to the sliding loads, and the elastic constants. The extension-kinking competition also involves  $\Gamma_s$  and  $\Gamma_i$ , the fracture resistances of the substrate and interface respectively. Broadly speaking, the tough substrate would confine the crack to extend along the interface. Kinking is favored if

$$\frac{\mathcal{G}^{\text{kink}}}{\mathcal{G}} > \frac{\Gamma_s}{\Gamma_i}. \quad (1)$$

The aim of the paper is to provide a comprehensive framework within which the material properties  $\Gamma_s$  and  $\Gamma_i$  can be quantified, and the driving forces  $\mathcal{G}^{\text{kink}}$  and  $\mathcal{G}$  can be computed, without ambiguity.

The plan of the paper is as follows. In Sections 2 and 3, we review the recently obtained general results on interface cracks. Effort is made to extend the interfacial fracture mechanics to include anisotropic solids, with special emphasis on orthotropic materials so that practical problems such as delamination of composites can be addressed. In Sections 4 and 5 the competition between crack extension along the interface and kinking into the substrate is formulated. Case studies are presented for bicrystals and aligned orthotropic bimetals. An explicit complex variable representation for orthotropic solids is summarized in Appendix A. The interaction solution for a dislocation and a crack, which is used as the kernel function for the integral equations, is presented in Appendix B.

## 2. CRACK TIP FIELD

Interface cracks in anisotropic solids were first analyzed by Gotoh (1967), Clements (1971) and Willis (1971). Recent results of Qu and Bassani (1989), Suo (1990) and Wu (1991) have made it possible to formulate a unified theory of a fracture toughness surface. Specifically, the structure of the interface crack tip field has been completely identified and analytical solutions have been found to several boundary value problems. The elasticity theory is summarized in this section using the notation of Suo (1990). The treatment is unified by a 3 by 3 positive definite Hermitian matrix,  $H$ , defined in Appendix A. The matrix depends on the elastic constants of the two materials and has dimension of compliance. Ting (1986) and Qu and Bassani (1989) showed that the oscillatory index  $\varepsilon = 0$  if and only if  $H$  is real. For this reason and several other considerations that will become clear, the real and

complex  $H$  are treated separately. As a convention, the crack lies on the  $(x, z)$  plane and propagates in the  $x$ -direction.

### 2.1. $H$ is real

For this case, the Hermitian matrix  $H$  becomes symmetric. Stresses are square root singular, and linear in three stress intensity factors  $K_I$ ,  $K_{II}$  and  $K_{III}$

$$\sigma_{ij} = \frac{1}{\sqrt{2\pi r}} [K_I \tilde{\sigma}_{ij}^I(\theta) + K_{II} \tilde{\sigma}_{ij}^{II}(\theta) + K_{III} \tilde{\sigma}_{ij}^{III}(\theta)]. \quad (2)$$

The dimensionless functions,  $\tilde{\sigma}_{ij}^I$ ,  $\tilde{\sigma}_{ij}^{II}$  and  $\tilde{\sigma}_{ij}^{III}$ , are so normalized that the interface tractions a distance  $r$  ahead of the tip take the familiar form

$$\sigma_{yy} = \frac{K_I}{\sqrt{2\pi r}}, \quad \sigma_{xy} = \frac{K_{II}}{\sqrt{2\pi r}}, \quad \sigma_{yz} = \frac{K_{III}}{\sqrt{2\pi r}}. \quad (3)$$

Suo (1990) noted that the angular functions in (2) are identical to those for a crack in homogeneous materials. Specifically, the functions for substrate 1 are the same as those for a crack in a homogeneous solid of the same elastic constants. The same holds for substrate 2. Consequently, these functions can be found in the article by Sih *et al.* (1965) on cracks in homogeneous anisotropic solids.

With the interface traction vector  $\mathbf{t} = \{\sigma_{yi}\} = \{\sigma_{yx}, \sigma_{yy}, \sigma_{yz}\}$ , the three stress intensity factors should be grouped as

$$\mathbf{k} = \{K_{II}, K_I, K_{III}\}. \quad (4)$$

In terms of  $\mathbf{k}$ , the near-tip traction vector can be rewritten

$$\mathbf{t}(r) = \frac{\mathbf{k}}{\sqrt{2\pi r}}. \quad (5)$$

The displacement jump vector,  $\boldsymbol{\delta} = \{\delta_x, \delta_y, \delta_z\}$ , a distance  $r$  behind the crack tip is linear in  $\mathbf{k}$ :

$$\boldsymbol{\delta}(r) = \sqrt{\frac{2r}{\pi}} H \mathbf{k}. \quad (6)$$

The energy release rate  $\mathcal{G}$  is quadratic in  $\mathbf{k}$ :

$$\mathcal{G} = \frac{1}{4} \mathbf{k}^T H \mathbf{k}. \quad (7)$$

Standard matrix operations are implied in the above formulae. The near-tip results given above were first obtained by Qu and Bassani (1989).

Analytic solutions have been found for several boundary value problems. An example is the Griffith crack of length  $L$  on the interface between two solids with real  $H$  but otherwise generally anisotropic. The body is subject to remote stresses  $\sigma_{yy}$ ,  $\sigma_{xy}$  and  $\sigma_{yz}$ . The stress intensity factors are:

$$K_I = \sigma_{yy} \sqrt{xL/2}, \quad K_{II} = \sigma_{xy} \sqrt{xL/2}, \quad K_{III} = \sigma_{yz} \sqrt{\pi L/2}. \quad (8)$$

It is understood that the appropriate stresses  $\sigma_{xx}$  and  $\sigma_{xz}$  are applied at infinity so that a uniform strain state exists at remote boundaries.

Two important classes of problems are known to have real  $H$ : (i) a crack in a homogeneous anisotropic solid (Sih *et al.*, 1965) and (ii) a crack along a tilt grain boundary with

the crack front *and* tilt axis normal to a mirror plane of the material (Qu and Bassani, 1989). In the following examples, the tensor  $H$  is given explicitly for orthotropic bimaternal, which are obtained by a simple rotation method described in Appendix A. All elastic constants are referred to the principal coordinate as defined in Appendix A.

*Example 1. Crack in a principal direction in a homogeneous orthotropic solid.* For a crack running in the principal direction  $x_1$ ,  $H$  is a diagonal matrix with elements

$$H_{11} = 4n(s_{11}s_{22})^{1/2}\lambda^{1/4}, \quad H_{22} = 4n(s_{11}s_{22})^{1/2}\lambda^{-1/4}, \quad H_{33} = 2(s_{44}s_{55})^{1/2}. \quad (9)$$

For example, the general expression (7) takes the explicit form

$$\mathcal{G} = \frac{1}{4}[H_{11}K_{II}^2 + H_{22}K_I^2 + H_{33}K_{III}^2]. \quad (10)$$

The order of the stress intensity factors is noted.

*Example 2. Crack in an arbitrary direction in a homogeneous orthotropic solid.* Consider a crack running in the direction  $x$ , which is rotated counterclockwise from the principal axis  $x_1$  by an angle  $\theta$ . The matrix  $H$  has elements

$$\begin{aligned} H_{11} &= 4n(s_{11}s_{22})^{1/2}(\lambda^{1/4}\cos^2\theta + \lambda^{-1/4}\sin^2\theta), \\ H_{22} &= 4n(s_{11}s_{22})^{1/2}(\lambda^{-1/4}\cos^2\theta + \lambda^{1/4}\sin^2\theta), \\ H_{12} &= H_{21} = -2n(s_{11}s_{22})^{1/2}(\lambda^{1/4} - \lambda^{-1/4})\sin 2\theta, \\ H_{33} &= 2(s_{44}s_{55})^{1/2}, \quad H_{13} = H_{23} = H_{31} = H_{32} = 0. \end{aligned} \quad (11)$$

*Example 3. Crack on a tilt grain boundary.* This is a bimaternal interface with real, symmetric  $H$ . The tilt boundary is formed by two misoriented, but otherwise identical, single crystals. The  $(x, y)$  plane is a plane of mirror symmetry and the crystal is orthotropic. The principal axis  $x_1$  of the two grains is rotated from the  $x$ -axis by  $\theta_1$  and  $\theta_2$ , respectively. For a crack on the grain boundary running in the  $x$ -direction, the elements of  $H$  are

$$\begin{aligned} H_{11} &= 2n(s_{11}s_{22})^{1/2}[(\cos^2\theta_1 + \cos^2\theta_2)\lambda^{1/4} + (\sin^2\theta_1 + \sin^2\theta_2)\lambda^{-1/4}], \\ H_{22} &= 2n(s_{11}s_{22})^{1/2}[(\cos^2\theta_1 + \cos^2\theta_2)\lambda^{-1/4} + (\sin^2\theta_1 + \sin^2\theta_2)\lambda^{1/4}], \\ H_{12} &= H_{21} = n(s_{11}s_{22})^{1/2}(\lambda^{1/4} - \lambda^{-1/4})(\sin 2\theta_1 - \sin 2\theta_2), \\ H_{33} &= 2(s_{44}s_{55})^{1/2}, \quad H_{13} = H_{23} = H_{31} = H_{32} = 0. \end{aligned} \quad (12)$$

## 2.2. $H$ is complex

The structure of the crack tip field is governed by an algebraic eigenvalue problem

$$\bar{H}\mathbf{w} = e^{2\pi\varepsilon} H\mathbf{w} \quad (13)$$

where  $\mathbf{w}$  is the eigenvector,  $e^{2\pi\varepsilon}$  the eigenvalue, and the overbar denotes the complex conjugate. The three distinct eigenpairs have the form  $(\varepsilon, \mathbf{w})$ ,  $(-\varepsilon, \bar{\mathbf{w}})$ ,  $(0, \mathbf{w}_3)$ . The oscillatory index  $\varepsilon$  is real, eigenvectors  $\mathbf{w}$  and  $\mathbf{w}_3$  are complex and real, respectively, and all of them are dimensionless. The physical significance of these quantities will be apparent shortly. For the case of real  $H$  consequences are clear:  $\varepsilon = 0$ , and any  $\mathbf{w}$  is an eigenvector. The eigenvectors  $\{1, 0, 0\}$ ,  $\{0, 1, 0\}$  and  $\{0, 0, 1\}$  are adopted in Section 2.1.

The crack tip field is a linear combination of two types of singularities; a coupled oscillatory field scaled by a complex  $K$ , and a non-oscillatory field scaled by a real  $K_3$ :

$$\sigma_{ij} = \frac{\operatorname{Re}\{Kr^{ie}\}}{\sqrt{2\pi r}} \tilde{\sigma}_{ij}^1(\theta) + \frac{\operatorname{Im}\{Kr^{ie}\}}{\sqrt{2\pi r}} \tilde{\sigma}_{ij}^2(\theta) + \frac{K_3}{\sqrt{2\pi r}} \tilde{\sigma}_{ij}^3(\theta). \quad (14a)$$

Here the dimensionless angular functions also depend on elastic constants and can be extracted from the near-tip solution in Suo (1990). The two stress intensities have different dimensions,

$$K = [\text{stress}][\text{length}]^{1/2-ie}, \quad K_3 = [\text{stress}][\text{length}]^{1/2}. \quad (14b)$$

The implications of the unusual dimensions will be explained later.

An essential step towards a unified concept of the *mode mixity* is to decompose the interfacial traction  $\mathbf{t} = \{\sigma_{yj}\}$  using eigenvectors as base vectors:

$$\mathbf{t} = t\mathbf{w} + \bar{t}\bar{\mathbf{w}} + t_3\mathbf{w}_3. \quad (15)$$

Here  $t$ ,  $\bar{t}$  and  $t_3$  are the *generalized components of the traction vector*, where  $t = t_2 + it_1$  is complex and  $t_3$  is real. Note in general  $t \neq \sigma_{yy} + i\sigma_{xy}$  and  $t_3 \neq t_{yz}$ . As  $r \rightarrow 0$ , the two components vary in accordance with

$$t(r) = \frac{Kr^{ie}}{\sqrt{2\pi r}}, \quad t_3(r) = \frac{K_3}{\sqrt{2\pi r}}. \quad (16)$$

Since  $r^{ie} = \exp(ie \ln r) = \cos(\varepsilon \ln r) + i \sin(\varepsilon \ln r)$ , the traction component  $t = t_2 + it_1$  rotates as  $r$  varies. The physical significance of  $\mathbf{w}$  and  $\mathbf{w}_3$  is now transparent. The component  $t_3$  projected onto  $\mathbf{w}_3$  is square root singular. In the plane spanned by  $\operatorname{Re}(\mathbf{w})$  and  $\operatorname{Im}(\mathbf{w})$ , the component  $t$  rotates and is square root singular.

The crack face displacement jump vector is

$$\delta(r) = (H + \bar{H}) \sqrt{\frac{r}{2\pi}} \left[ \frac{Kr^{ie}\mathbf{w}}{(1+2ie)\cosh \pi\varepsilon} + \frac{\bar{K}r^{-ie}\bar{\mathbf{w}}}{(1-2ie)\cosh \pi\varepsilon} + K_3\mathbf{w}_3 \right]. \quad (17)$$

The energy release rate is related to  $K$  and  $K_3$  via

$$\mathcal{G} = \frac{\bar{\mathbf{w}}^T(H + \bar{H})\mathbf{w}}{4 \cosh^2 \pi\varepsilon} |K|^2 + \frac{1}{8} \mathbf{w}_3^T(H + \bar{H})\mathbf{w}_3 K_3^2. \quad (18)$$

Note the contributions from the two types of singularities are additive. These near-tip fields were first obtained by Suo (1990).

To date, only one class of boundary value problems has been analyzed for generally anisotropic materials, namely a colinear array of cracks on the interface between two semi-infinite substrates. The stress intensity factors are found to be identical to their counterparts for isotropic bimetals. For example, for the Griffith crack described earlier, with the applied traction vector  $\mathbf{t} = \{\sigma_{yx}, \sigma_{yy}, \sigma_{yz}\}$  decomposed into the generalized components  $t$  and  $t_3$ , the solution is

$$K = t(1+2ie)L^{-ie}\sqrt{\pi L/2}, \quad K_3 = t_3\sqrt{\pi L/2}. \quad (19)$$

This is formally identical to the solution for isotropic bimetals. However, in general  $t \neq \sigma_{yy} + i\sigma_{yx}$  and  $t_3 \neq \sigma_{yz}$ . Contrasted below are the near-tip field structures for isotropic and orthotropic bimetals.

*Example 1. Isotropic bimaterial.* For an interface crack between two isotropic materials, the  $H$  matrix takes the form

$$H = \frac{4}{E^*} \begin{bmatrix} 1 & -i\beta & 0 \\ i\beta & 1 & 0 \\ 0 & 0 & E^*/2\mu^* \end{bmatrix} \quad (20)$$

where, for plane strain,

$$\frac{2}{E^*} = \frac{1-\nu_1^2}{E_1} + \frac{1-\nu_2^2}{E_2}, \quad \frac{2}{\mu^*} = \frac{1}{\mu_1} + \frac{1}{\mu_2}$$

$$\alpha = \frac{\mu_1(1-\nu_2) - \mu_2(1-\nu_1)}{\mu_1(1-\nu_2) + \mu_2(1-\nu_1)}, \quad \beta = \frac{1}{2} \frac{\mu_1(1-2\nu_2) - \mu_2(1-2\nu_1)}{\mu_1(1-\nu_2) + \mu_2(1-\nu_1)}. \quad (21)$$

The bielastic constants  $\alpha$  and  $\beta$  are called Dundurs' parameters. From (13), the eigenvalue and eigenvectors are

$$\varepsilon = \frac{1}{2\pi} \ln \frac{1-\beta}{1+\beta}, \quad \mathbf{w} = \{-i/2, 1/2, 0\}, \quad \mathbf{w}_3 = \{0, 0, 1\}. \quad (22)$$

It follows from (15) that the two traction components take the familiar form

$$t = \sigma_{yy} + i\sigma_{xy}, \quad t_3 = \sigma_{yz}. \quad (23)$$

The stress intensity factors,  $K$  and  $K_3$ , are defined such that the two traction components a distance  $r$  ahead of the crack tip are scaled as

$$\sigma_{yy} + i\sigma_{xy} = \frac{Kr^{i\varepsilon}}{\sqrt{2\pi r}}, \quad \sigma_{yz} = \frac{K_3}{\sqrt{2\pi r}}. \quad (24)$$

The displacement jumps a distance  $r$  behind the crack tip are

$$\delta_y + i\delta_x = \frac{1}{(1+2i\varepsilon) \cosh \pi\varepsilon} \frac{4Kr^{i\varepsilon}}{E^*} \sqrt{\frac{2r}{\pi}}, \quad \delta_z = \frac{2K_3}{\mu^*} \sqrt{\frac{2r}{\pi}}. \quad (25)$$

The energy release rate is related to  $K$  and  $K_3$  by

$$\mathcal{G} = \frac{|K|^2}{E^* \cosh^2 \pi\varepsilon} + \frac{1}{2\mu^*} K_3^2. \quad (26)$$

*Example 2. Aligned orthotropic bimaterial.* Consider two dissimilar orthotropic materials bonded with the principal axes aligned, and the interface is running in the  $x_1$ -direction. The components of  $H$  are

$$\begin{aligned} H_{11} &= [2n\lambda^{1/4} \sqrt{s_{11}s_{22}}]_1 + [2n\lambda^{1/4} \sqrt{s_{11}s_{22}}]_2 \\ H_{22} &= [2n\lambda^{-1/4} \sqrt{s_{11}s_{22}}]_1 + [2n\lambda^{-1/4} \sqrt{s_{11}s_{22}}]_2 \\ H_{12} &= \bar{H}_{21} = i[\sqrt{s_{11}s_{22} + s_{12}}]_1 - i[\sqrt{s_{11}s_{22} + s_{12}}]_2 \\ H_{33} &= [\sqrt{s_{44}s_{55}}]_1 + [\sqrt{s_{44}s_{55}}]_2 \\ H_{13} &= H_{23} = H_{31} = H_{32} = 0. \end{aligned} \quad (27)$$

Here  $[ ]_1$  designates quantities for material 1, and  $[ ]_2$  for material 2. The generalized Dundurs' parameters  $\alpha$  and  $\beta$  are given by

$$\alpha = (\Sigma - 1)/(\Sigma + 1), \quad \beta = iH_{12}(H_{11}H_{22})^{-1/2} \quad (28)$$

where  $\Sigma = [\sqrt{s_{11}s_{22}}]_2/[\sqrt{s_{11}s_{22}}]_1$ . The solution to the eigenvalue problem (13) is

$$\varepsilon = \frac{1}{2\pi} \ln \frac{1-\beta}{1+\beta}, \quad \mathbf{w} = \left\{ -\frac{i}{2} \sqrt{\frac{H_{22}}{H_{11}}}, \frac{1}{2}, 0 \right\}, \quad \mathbf{w}_3 = \{0, 0, 1\}. \quad (29)$$

It follows from (15) that the generalized traction components are

$$t = \sigma_{yy} + i \sqrt{\frac{H_{11}}{H_{22}}} \sigma_{xy}, \quad t_3 = \sigma_{zy}. \quad (30)$$

Note that the complex component now contains a scaling factor. For example, for most polymeric composites with cross-ply laminates  $\sqrt{H_{11}/H_{22}}$  is between 1 and 2. The near-tip stress field consists of two types of singularities: an oscillatory singularity scaled by the complex  $K$ , and a square root singularity scaled by  $K_3$ ,

$$\sigma_{yy} + i \sqrt{\frac{H_{11}}{H_{22}}} \sigma_{xy} = \frac{Kr^{i\varepsilon}}{\sqrt{2\pi r}}, \quad \sigma_{zy} = \frac{K_3}{\sqrt{2\pi r}}. \quad (31)$$

Observe that the complex stress intensity factor  $K$  does not reduce to  $K_I + iK_{II}$  when  $\varepsilon = 0$ . If and only if  $H_{11}/H_{22} = 1$  do the stress intensity factors  $K$  reduce to the conventional stress intensity factors. The above normalization of  $K$  is slightly different from that introduced by Suo (1990).

The displacement jumps have the form

$$\delta_y + i \sqrt{\frac{H_{22}}{H_{11}}} \delta_x = \frac{H_{22}Kr^{i\varepsilon}}{(1+2i\varepsilon) \cosh \pi\varepsilon} \sqrt{\frac{2r}{\pi}}, \quad \delta_z = H_{33}K_3 \sqrt{\frac{2r}{\pi}}. \quad (32)$$

The Irwin-type energy release rate is

$$\mathcal{G} = \frac{H_{22}}{4 \cosh^2 \pi\varepsilon} |K|^2 + \frac{1}{4} H_{33} K_3^2. \quad (33)$$

*Example 3. Misaligned orthotropic bimaterial.* The explicit form of  $H$  can be obtained from the  $B$ -matrix (A11) in Appendix A. Details are omitted here.

### 3. MODE MIXITY AND SURFACE TOUGHNESS

It has been generally observed in experiments that cracks in isotropic, homogeneous, brittle solids seek to propagate on planes ahead of which local Mode I conditions prevail. Consequently, one single parameter,  $K_{IC}$ , can be designated to each material to quantify its resistance to fracture. By contrast, whenever planes of low fracture resistance exist, cracks may be trapped onto such planes, regardless of the local mode mixity. Orthotropic materials such as composites and brittle crystals provide examples where definite weak planes exist: longitudinal planes for composites and cleavage planes for crystals. Interfaces offer another example when they are brittle compared with the substrates. A well-documented experimental fact is that fracture resistance for such weak planes depend strongly on mode mixity. Rather than a single toughness value, it is values at various mode mixities that fully characterize the fracture resistance of a weak plane. In the following paragraphs, mode mixity will be defined precisely for both  $H$  real and  $H$  complex.

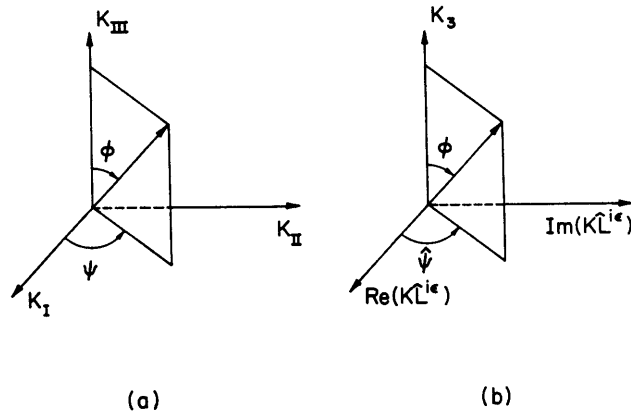


Fig. 2. Mode mixities defined as solid angles in the  $K$  space.

### 3.1. Mode mixity for material pairs with real $H$

When all three modes are present, the mode mixity is fully specified by two solid angles,  $\psi$  and  $\phi$ , in the space of the interface traction vector  $\mathbf{t} = \{\sigma_{yx}, \sigma_{yy}, \sigma_{yz}\}$ ,

$$\tan \psi = \sigma_{xy}/\sigma_{yy}, \quad \cos \phi = \sigma_{yz}/|\mathbf{t}| \quad \text{as } r \rightarrow 0. \quad (34)$$

With the asymptotic field (3), an equivalent definition can be given in the  $(K_I, K_{II}, K_{III})$  space:

$$\tan \psi = \frac{K_{II}}{K_I}, \quad \cos \phi = \frac{K_{III}}{(K_I^2 + K_{II}^2 + K_{III}^2)^{1/2}}. \quad (35)$$

The mixities  $\psi$  and  $\phi$  are indicated in Fig. 2a. These definitions also apply to cracks in homogeneous materials.

For a given mode mixity  $\phi$  and  $\psi$ , the fracture toughness,  $\Gamma$ , is defined as the energy release rate  $\mathcal{G}$  at the onset of crack growth. The fracture toughness,  $\Gamma(\psi, \phi)$  is a property of the bimaterial interface. For a given bimaterial interface, it is a surface in the  $K$  space, which in general should be determined directly by experiments. Upon loading, a crack will not propagate unless the driving force reaches the surface toughness, i.e. the mixed mode fracture condition is

$$\mathcal{G}(\psi, \phi) = \Gamma(\psi, \phi). \quad (36)$$

In the composite community, mode mixity is specified by the ratio  $\mathcal{G}_{II}/\mathcal{G}_I$ . For a crack running along the principal axis in an orthotropic material, this ratio is equivalent, but not identical, to mode mixity  $\psi$  defined here [see (35)]. In general, however, this ‘‘energetic’’ mode mixity is not advised since  $\mathcal{G}_I$  and  $\mathcal{G}_{II}$  cannot be unambiguously defined.

### 3.2. Mode mixity for material pairs where $H$ is complex

The mode mixity concept can be extended to oscillatory fields by using the generalized traction components  $t = t_2 + it_1$  and  $t_3$  in (15):

$$\tan \hat{\psi} = \left( \frac{t_1}{t_2} \right)_{r=\hat{L}}, \quad \cos \hat{\phi} = \left( \frac{t_3}{|\mathbf{t}|} \right)_{r \rightarrow 0}. \quad (37)$$

Here it is necessary to introduce a fixed length  $\hat{L}$  in order that the mode mixity be uniquely specified.  $\hat{L}$  must be independent of the overall specimen size and specimen types; a sensible choice of  $\hat{L}$  should fall between the inelastic zone size and the specimen size. For example,  $\hat{L} = 100 \mu\text{m}$  is suitable for many brittle bimaterial specimens at the laboratory scale.



Using the asymptotic field (16), the mode mixities  $\hat{\psi}$  and  $\phi$  can also be defined in the  $K$  space

$$K\hat{L}^{ie} = |K| e^{i\hat{\psi}}, \quad \cos \phi = \frac{K_3}{\sqrt{|K|^2 + K_3^2}}. \quad (38)$$

The mode mixities  $\hat{\psi}$  and  $\phi$  are indicated in Fig. 2b. As a consequence of the oscillatory field, the traction ratio  $t_1/t_2$  varies *slowly* as  $r$  moves away from the tip. As implied by (38), the phase shift from  $r = \hat{L}_1$  to  $r = \hat{L}_2$  is

$$\hat{\psi}_2 - \hat{\psi}_1 = \varepsilon \ln(\hat{L}_2/\hat{L}_1). \quad (39)$$

This would not be a big shift for moderate variations in  $\hat{L}$ . For example, for a glass–alumina interface,  $\varepsilon = 0.05$ , the phase shift for a decade change  $\hat{L}_2/\hat{L}_1 = 10$  is  $\hat{\psi}_2 - \hat{\psi}_1 = 6.6^\circ$ .

The mixed mode fracture condition is

$$\mathcal{G}(\hat{\psi}, \phi) = \Gamma(\hat{\psi}, \phi). \quad (40)$$

The fracture resistance is unambiguously specified by a surface  $\Gamma(\hat{\psi}, \phi)$ , together with a length  $\hat{L}$  for the definition of  $\hat{\psi}$ . This engineering approach to quantify the fracture resistance is an extension of the existing theory for isotropic solids. The conceptual basis for this approach is summarized in Rice (1988) and several articles in a volume edited by Rühle *et al.* (1990). The experimental implementation can be found in Wang and Suo (1990), Liechti and Chai (1991), and Ahmad and Majumdar (1991).

Consider the loading phase  $\hat{\psi}$  for two special cases. For an isotropic bimaterial

$$\tan \hat{\psi} = \frac{\text{Im}(K\hat{L}^{ie})}{\text{Re}(K\hat{L}^{ie})} = \left( \frac{\sigma_{yz}}{\sigma_{yy}} \right)_{r=\hat{L}} \quad (41)$$

and for an aligned orthotropic bimaterial

$$\tan \hat{\psi} = \frac{\text{Im}(K\hat{L}^{ie})}{\text{Re}(K\hat{L}^{ie})} = \sqrt{\frac{H_{11}}{H_{22}}} \left( \frac{\sigma_{yx}}{\sigma_{yy}} \right)_{r=\hat{L}}. \quad (42)$$

The scaling factor  $\sqrt{H_{11}/H_{22}}$  is necessary to maintain the phase shift rule (39), which is important in interpreting and using surface toughness.

### 3.3. Experimental determination of surface toughnesses

In principle any geometry with an interface crack can be used to determine toughness. The geometry can be calibrated by analytical or numerical evaluation of the stress intensity factors. As an example, consider a Griffith crack of length  $L$  on the interface between two aligned orthotropic materials. Specialized from (19), the complex stress intensity factor is

$$K = (1 + 2i\varepsilon)\sqrt{\pi L/2L}^{-ie}(\sigma_{yy} + i\sqrt{H_{11}/H_{22}}\sigma_{xy}). \quad (43)$$

The loading phase  $\hat{\psi}$ , extracted by comparing (43) with its definition in (38), is

$$\hat{\psi} = \tan^{-1}(2\varepsilon) + \tan^{-1}\left(\sqrt{\frac{H_{11}}{H_{22}}}\frac{\sigma_{xy}}{\sigma_{yy}}\right) + \varepsilon \ln\left(\frac{\hat{L}}{L}\right). \quad (44)$$

The last term is the phase change with crack size  $L$  under fixed applied load.

The mode mixity can be varied either by changing the proportion of the loads for multi-load specimens or by the change of specimen configuration. A set of specimens which

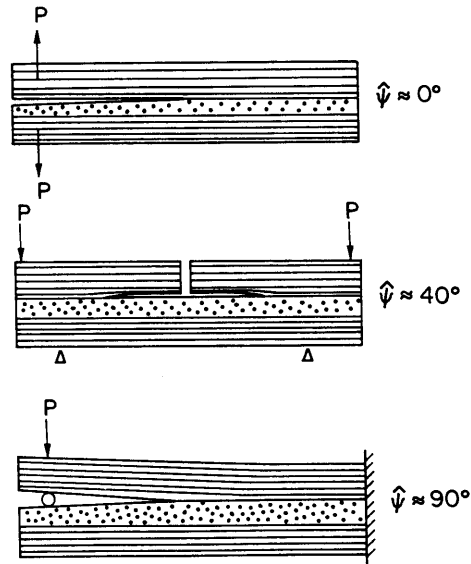


Fig. 3. Schematic of specimens for the determination of mixed mode delamination toughness for cross-ply laminates.

is suitable for cross-ply composites is illustrated in Fig. 3. These geometries produce near-tip fields ranging from predominantly tension to predominantly shear. They are calibrated using finite element analysis by Choi *et al.* (1991). Similar specimens for uniaxial composites have been calibrated by Bao *et al.* (1991) for arbitrary elastic constants.

#### 4. KINKING IN BICRYSTALS

The topic of crack kinking is now taken up. Figure 4 shows a tilt grain boundary of an orthotropic crystal, i.e. the two grains are misoriented but otherwise identical. The principal material axis  $x_1$  is tilted from  $x$  by angles  $\theta_1$  and  $\theta_2$ , respectively. The  $(x, y)$  plane is a plane of mirror symmetry, and the tilt axis and crack front are normal to the  $(x, y)$  plane. A small scale kinking problem is considered in that the kink length  $a$  is the only length scale in the problem, i.e., all the other lengths are much larger than the kink length. As noted in example 3 in Section 2.1, the matrix  $H$  for such a grain boundary crack is real,

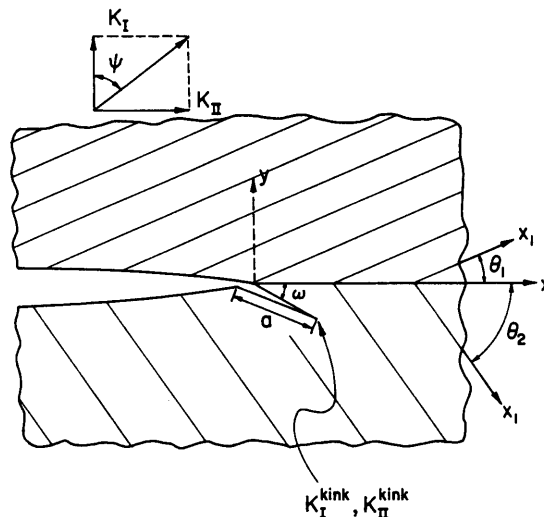


Fig. 4. A schematic of a small-scale kink problem. The principal direction  $x_1$  is tilted from the  $x$ -axis by  $\theta_1$  and  $\theta_2$  respectively. The parent crack is under mixed mode load.

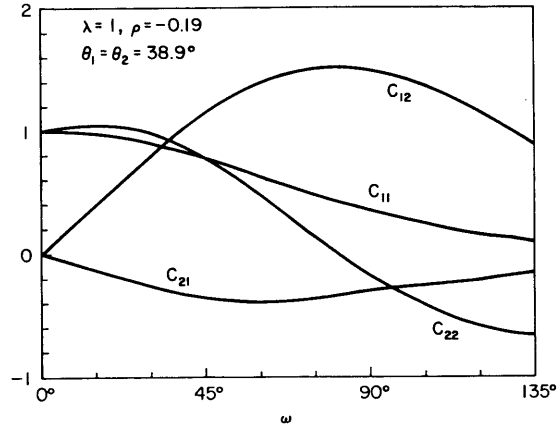


Fig. 5. Coefficients  $C_{ij}$  for a symmetric tilt cubic bicrystal.

and the crack tip field is non-oscillatory, square root singular. Consequently, the remote loading can be specified by the stress intensity factors  $K_I$  and  $K_{II}$  of the familiar type. Consistent with the spirit of the small-scale kinking formulation,  $K_I$  and  $K_{II}$  should be computed from the actual specimen size and loading with the kink ignored. The stress intensity factors at the kink tip are denoted by  $K_I^{\text{kink}}$  and  $K_{II}^{\text{kink}}$ .

Linearity and dimensionality dictate that

$$\begin{aligned} K_I^{\text{kink}} &= C_{11}K_I + C_{12}K_{II} \\ K_{II}^{\text{kink}} &= C_{21}K_I + C_{22}K_{II} \end{aligned} \quad (45)$$

where  $C_{ij}$  depend on  $\omega$ ,  $\theta_1$ ,  $\theta_2$ ,  $\lambda$  and  $\rho$  but *not* on kink length  $a$ . The complete solution for a special problem, crack deflection in homogeneous orthotropic solids, has been reported elsewhere (Suo *et al.*, 1991). Determination of these coefficients requires that the boundary layer problem be solved rigorously. An integral equation method used in He and Hutchinson (1989) was adopted; the kernel function needed for this work is presented in Appendix B. Attention here is restricted to several case studies that reveal the effect of anisotropy.

#### 4.1. Cubic bicrystals

Consider two cubic crystals with elastic constants  $\lambda = 1$  and  $\rho = -0.19$  which form a symmetric tilt grain boundary with  $\theta_1 = \theta_2 = 38.9^\circ$  (Fig. 4). The computed values of  $C_{ij}$  as a function of the kink angle  $\omega$  are shown in Fig. 5.

The energy release rate for the crack extending along the interface, specialized from (12) and (7), is

$$\mathcal{G} = s_{11}n[K_I^2 + K_{II}^2]. \quad (46)$$

For the kinked crack,  $\mathcal{G}^{\text{kink}}$  can be obtained from (10) by setting  $\lambda = 1$  and  $s_{11} = s_{22}$ :

$$\mathcal{G}^{\text{kink}} = s_{11}n[(K_I^{\text{kink}})^2 + (K_{II}^{\text{kink}})^2]. \quad (47)$$

Note that energy release rate relations are identical in form: a consequence of  $H$  being anisotropic second order tensor for subic bimerials. The ratio  $\mathcal{G}^{\text{kink}}/\mathcal{G}$  is plotted as a

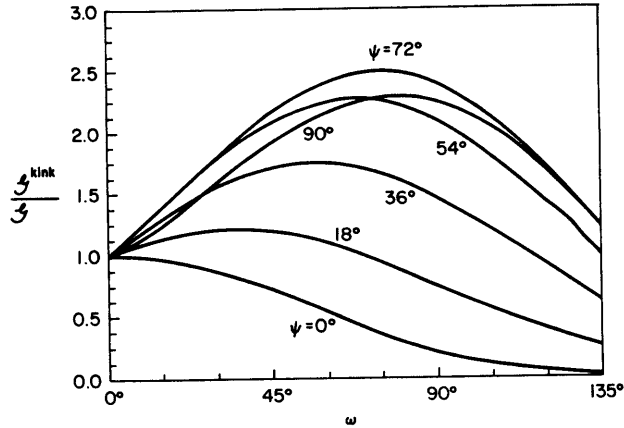


Fig. 6. Crack driving force ratios  $\mathcal{G}^{\text{kink}}/\mathcal{G}$  as a function of the kink angle  $\omega$  under several remote loading mixities  $\psi = \tan^{-1}(K_{II}/K_I)$ .

function of kink angle  $\omega$  for several values of remote loading phase  $\psi$  in Fig. 6. Since the parent crack is mostly likely to kink into a principal plane, i.e.  $\omega = \theta_2$ , we have cross-plotted the ratio  $\mathcal{G}^{\text{kink}}/\mathcal{G}$  as a function of loading phase  $\psi$  for  $\omega = \theta_2 = 38.9^\circ$  in Fig. 7. The curve clearly shows that the available energy for kinking increases rapidly and then decreases with the loading phase. As a comparison, the result from He and Hutchinson (1989) for isotropic material ( $\rho = 1$ ) is included in the plot. The effect of anisotropy can be seen; the isotropic approximation would underestimate the possibility of kinking.

The additional information required to assess the competition between extension and kinking is the fracture resistances of the substrate and the interface,  $\Gamma_s$  and  $\Gamma_i$ . Thus kinking is favored if  $\mathcal{G}^{\text{kink}}/\mathcal{G} > \Gamma_s/\Gamma_i$ .

4.2. Orthotropic bicrystals

The orthotropy parameters are taken to be  $\lambda = 0.338$  and  $\rho = 0.439$  for this case study. The principal axes of the top and bottom crystals are rotated by  $\theta_1 = 30^\circ$  and  $\theta_2 = 75^\circ$ , respectively. The computed values of  $C_{ij}$  are plotted in Fig. 8.

The energy release rates are computed from stress intensity factors using the Irwin-type expressions given in Section 2.1. Figure 9 shows the ratio  $\mathcal{G}^{\text{kink}}/\mathcal{G}$  as a function of loading phase  $\psi$  for  $\omega = \theta_2 = 75^\circ$ . For comparison purposes, the result from He and Hutchinson (1989) is included in the plot. The effect of anisotropy can be seen; the possibility of kinking is also underestimated by the isotropic approximation.

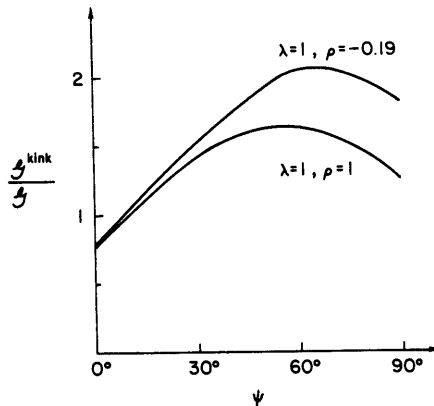
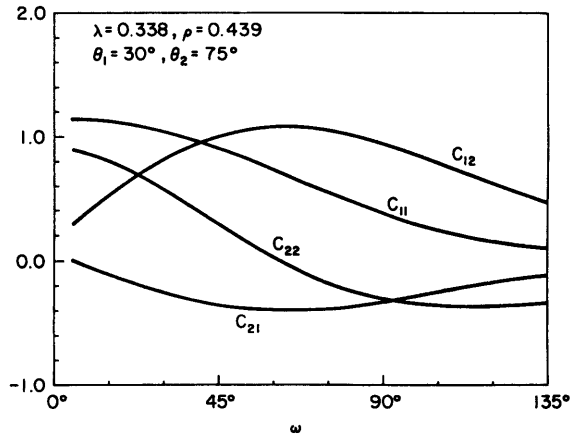
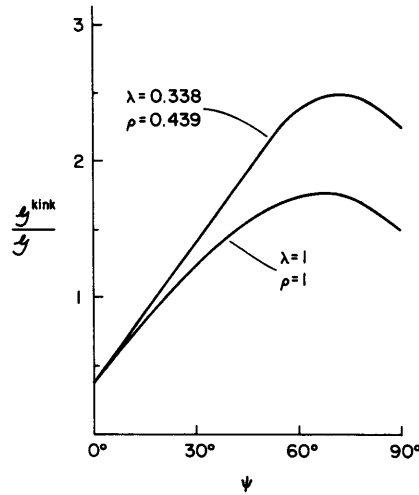


Fig. 7. Comparison of the crack driving force ratio  $\mathcal{G}^{\text{kink}}/\mathcal{G}$  between isotropic ( $\rho = 1$ ) and cubic ( $\rho = -0.19$ ) bicrystals.

Fig. 8. Coefficients  $C_{ij}$  for an orthotropic bicrystal.Fig. 9. Crack driving force ratios  $G^{\text{kink}}/G$  for orthotropic and isotropic bicrystals. The discrepancy is clearly seen.

### 5. KINKING IN ALIGNED ORTHOTROPIC BIMATERIALS

Consider a parent crack on the interface between dissimilar orthotropic materials but bonded with aligned principal axes. As discussed in Section 2.2, the stress field at such an interface crack tip is oscillatory and square root singular. A small-scale kinking problem is formulated with remote applied load represented by a complex stress intensity factor  $K$  (Fig. 10). By dimensional analysis, the stress intensity factors at the kink tip are:

$$\begin{aligned} K_I^{\text{kink}} &= C_{11} \operatorname{Re}(Ka^{ie}) + C_{12} \operatorname{Im}(Ka^{ie}) \\ K_{II}^{\text{kink}} &= C_{21} \operatorname{Re}(Ka^{ie}) + C_{22} \operatorname{Im}(Ka^{ie}) \end{aligned} \quad (48)$$

where  $C_{ij}$  depend on the kink angle  $\omega$  and elastic constants but not on kink size  $a$ . Since  $K$  has the generic structure  $K = |K| e^{i\hat{\psi}} \hat{L}^{-ie}$  the above relations can be rewritten more explicitly:

$$\begin{aligned} K_I^{\text{kink}} &= |K| \left[ C_{11} \cos\left(\hat{\psi} + \varepsilon \ln \frac{a}{\hat{L}}\right) + C_{12} \sin\left(\hat{\psi} + \varepsilon \ln \frac{a}{\hat{L}}\right) \right] \\ K_{II}^{\text{kink}} &= |K| \left[ C_{21} \cos\left(\hat{\psi} + \varepsilon \ln \frac{a}{\hat{L}}\right) + C_{22} \sin\left(\hat{\psi} + \varepsilon \ln \frac{a}{\hat{L}}\right) \right]. \end{aligned} \quad (49)$$

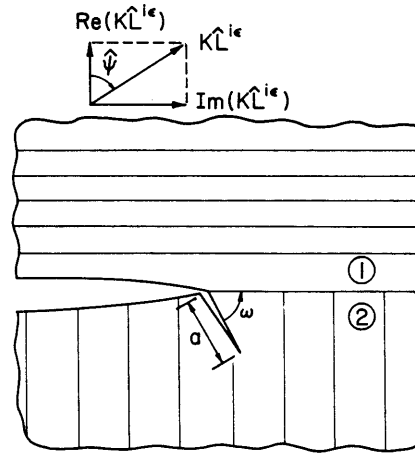


Fig. 10. An aligned orthotropic bimaterial is under remote mixed mode load. The parent crack kinks into material 2.

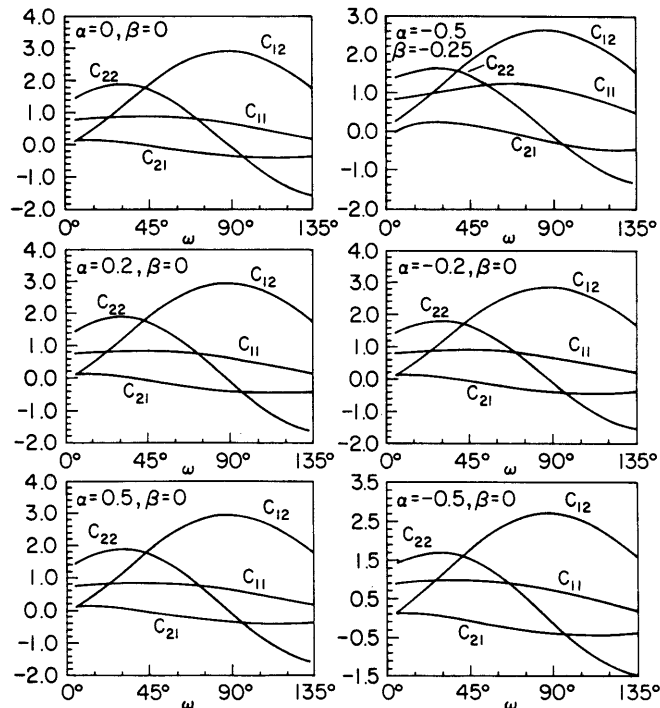


Fig. 11. Coefficients  $C_{ij}$  for aligned orthotropic solids ( $\lambda_1 = 1.0$ ,  $\rho_1 = 0.19$ ,  $\lambda_2 = 0.12$ ,  $\rho_2 = 6.4$ ).

The elastic constants for the two materials are taken to be  $\lambda_1 = 1.0$ ,  $\rho_1 = 0.19$ ,  $\lambda_2 = 0.12$ ,  $\rho_2 = 6.4$ . The values for  $C_{ij}$  are plotted in Fig. 11 for six different combinations of  $\alpha$  and  $\beta$ . The ratio  $\mathcal{G}^{\text{kink}}/\mathcal{G}$  as a function of phase angle  $\hat{\psi} + \epsilon \ln(a/\hat{L})$ , all with  $\omega = 90^\circ$  is plotted in Fig. 12. The role of elastic mismatch parameters  $\alpha$  and  $\beta$  are clearly shown. We point out that the phase angle in (49) is based on a fixed length  $\hat{L}$  which is independent of the specimen size. For example,  $\hat{L}$  could be chosen to be comparable in magnitude with defect size  $a$  so that the term  $\epsilon \ln(a/\hat{L})$  is negligible. This treatment is consistent with the mixed mode toughness concept discussed in Section 3, and avoids the conceptual difficulties that arise in He and Hutchinson (1989).

## 6. CONCLUDING REMARKS

A comprehensive framework to assess whether cracks extend along, or kink out of, interfaces has been formulated. The framework makes advantageous use of several unifying

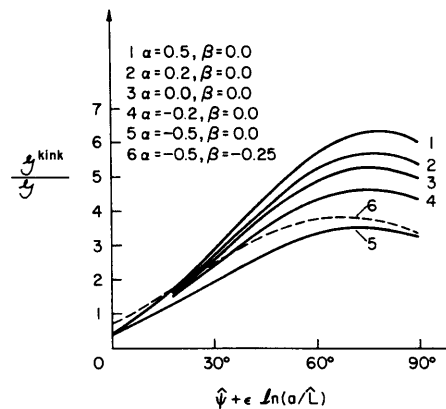


Fig. 12. The ratio  $\mathcal{G}^{\text{kink}}/\mathcal{G}$  as a function of the loading phase  $\hat{\psi} + \epsilon \ln(\hat{L}/a)$  for  $\omega = 90^\circ$  kink.

concepts: the  $H$  tensor, eigenvectors  $\mathbf{w}$  and  $\mathbf{w}_3$ , generalized interfacial traction components  $t$  and  $t_3$ , and mode mixity  $\hat{\psi}$  and  $\phi$ . The framework is completely general in that no special material symmetry is assumed. The explicit results tabulated for orthotropic bimetals allow immediate applications to bicrystals and cross-ply laminates. Several crack geometries, which are suitable for evaluating the fracture resistance of uniaxial and cross-ply composites, have been calibrated (Bao *et al.*, 1990; Choi *et al.*, 1990). Many more mixed mode specimen calibrations and fracture testings are needed before a fully rationalized composite material characterization can be accomplished.

*Acknowledgements*—T.C.W. and C.F.S. are supported by the Office of Naval Research through ONR Grant “Mechanics of Interfacial Fracture”. Z.S. is supported by an NSF research initiative award (MSS-9011571), and by an ONR/URI contract (N00014-86-K-0753). The computations were carried out at the Computational Mechanics Research Facility within the Division of Engineering of Brown University.

#### REFERENCES

- Ahmad, J. and Majumdar, B. S. (1991). An engineering fracture mechanics analysis of metal/ceramic and ceramic/ceramic joints (submitted for publication).
- Bao, G., Ho, S., Fan, B. and Suo, Z. (1991). The role of material orthotropy in fracture specimens for composites (submitted for publication).
- Cao, H. C. and Evans, A. G. (1989). An experimental study of the fracture resistance of bimaterial interface. *Mech. Mater.* **7**, 295–305.
- Charalambides, P. G., Lund, J., Evans, A. G. and McMeeking, R. M. (1989). A test specimen for determining the fracture resistance of bimaterial interface. *J. Appl. Mech.* **56**, 77–82.
- Choi, H. C., Shih, C. F. and Suo, Z. (1991). Specimens to determine mixed mode delamination toughness for cross-ply laminates (work in progress).
- Clements, D. L. (1971). A crack between dissimilar anisotropic media. *Int. J. Engng Sci.* **9**, 257–265.
- Eshelby, J. D., Read, W. T. and Shockley, W. (1953). Anisotropic elasticity with applications to dislocation theory. *Acta Metall.* **1**, 251–259.
- Gotoh, M. (1967). Some problems of bonded anisotropic plates with cracks along the bond. *Int. J. Fracture Mech.* **3**, 253–260.
- He, M. Y. and Hutchinson, J. W. (1989). Kinking of a crack out of an interface. *J. Appl. Mech.* **56**, 270–278.
- Hutchinson, J. W. and Suo, Z. (1991). Mixed mode cracking in layered materials. In *Advances in Applied Mechanics*, Vol. 28. Academic Press, New York (in press).
- Lekhnitskii, S. G. (1981). *Theory of Elasticity of an Anisotropic Body*. Mir Publishers, Moscow.
- Liechti, K. M. and Chai, Y.-S. (1991). Biaxial loading experiments for determining interfacial fracture toughness. *J. Appl. Mech.* (in press).
- O’Dowd, N. P., Shih, C. F. and Stout, M. (1990). Test geometries for measuring interfacial fracture toughness. *Int. J. Solids Structures* (to appear).
- Qu, J. and Bassani, J. L. (1989). Cracks on bimaterial and bicrystal interfaces. *J. Mech. Phys. Solids* **37**, 417–433 (see also an accompanying paper by the authors in the same issue).
- Rice, J. R. (1988). Elastic fracture mechanics concepts for interfacial cracks. *J. Appl. Mech.* **55**, 98–103.
- Ruhle, M., Evans, A. G., Ashby, M. F. and Hirth, J. P. (1990). *Metal–Ceramic Interfaces*, *Acta Scripta Metallurgica Proceedings Series 4*. Pergamon Press, New York.
- Sih, G. C., Paris, P. C. and Irwin, G. R. (1965). On cracks in rectilinearly anisotropic bodies. *Int. J. Fracture Mech.* **1**, 189–203.
- Stroh, A. N. (1958). Dislocations and cracks in anisotropic elasticity. *Phil. Mag.* **7**, 625–646.
- Suo, Z. (1990). Singularities, interfaces and cracks in dissimilar anisotropic media. *Pro. R. Soc. Lond. A* **427**, 331–358.

- Suo, Z. and Hutchinson, J. W. (1989). Sandwich test specimens for measuring interface crack toughness. *Mater. Sci. Engng A* **107**, 135–143.
- Suo, Z., Bao, G., Fan, B. and Wang, T. C. (1991). Orthotropy rescaling and implications for fracture in composites. *Int. J. Solids Structures* **28**(2), 235–248.
- Ting, T. C. T. (1982). Effects of change of reference coordinates on the stress analyses of anisotropic elastic materials. *Int. J. Solids Structures* **18**, 139–152.
- Ting, T. C. T. (1986). Explicit solution and invariance of the singularities at an interface crack in anisotropic composites. *Int. J. Solids Structures* **22**, 965–983.
- Wang, J. S. and Suo, Z. (1990). Experimental determination of interfacial toughness curves using Brazilian-nut-sandwiches. *Acta Metall.* **38**, 1279–1290.
- Willis, J. R. (1971). Fracture mechanics of interfacial cracks. *J. Mech. Phys. Solids* **19**, 353–368.
- Wu, K. C. (1991). Stress intensity factor and energy release rate for interfacial cracks between dissimilar anisotropic materials. *J. Appl. Mech.* (in press).

#### APPENDIX A: COMPLEX VARIABLE REPRESENTATION FOR ORTHOTROPIC MATERIALS

For many problems of practical interest, each of the two bonded materials is orthotropic but their principal axes may not be aligned. The stress–strain relation in the principal coordinates is:

$$\begin{pmatrix} \epsilon_{11} \\ \epsilon_{22} \\ \epsilon_{33} \\ 2\epsilon_{23} \\ 2\epsilon_{31} \\ 2\epsilon_{12} \end{pmatrix} = \begin{bmatrix} s_{11} & s_{12} & s_{13} & 0 & 0 & 0 \\ s_{21} & s_{22} & s_{23} & 0 & 0 & 0 \\ s_{31} & s_{32} & s_{33} & 0 & 0 & 0 \\ 0 & 0 & 0 & s_{44} & 0 & 0 \\ 0 & 0 & 0 & 0 & s_{55} & 0 \\ 0 & 0 & 0 & 0 & 0 & s_{66} \end{bmatrix} \begin{pmatrix} \sigma_{11} \\ \sigma_{22} \\ \sigma_{33} \\ \sigma_{23} \\ \sigma_{31} \\ \sigma_{12} \end{pmatrix}. \quad (\text{A1})$$

Here  $s_{ij}$  are compliances which are related to the Young's moduli, shear modulus and Poisson's ratios, e.g.,  $s_{11} = 1/E_1$ ,  $s_{22} = 1/E_2$ ,  $s_{66} = 1/G_{12}$  and  $s_{12} = -\nu_{12}/E_1 = -\nu_{21}/E_2$ .

As observed in Suo (1990), the in-plane stress fields depend on two dimensionless parameters,

$$\lambda = \frac{s_{11}}{s_{22}} = \frac{E_2}{E_1}, \quad \rho = \frac{2s_{12} + s_{66}}{2(s_{11}s_{22})^{1/2}} = \frac{(E_1E_2)^{1/2}}{2G_{12}} - (\nu_{12}\nu_{21})^{1/2}. \quad (\text{A2})$$

They measure the in-plane orthotropy:  $\lambda = \rho = 1$  for isotropic solids and  $\lambda = 1$  for solids with cubic symmetry. Ellipticity implies that  $\lambda > 0$  and  $\rho > -1$ . Values for representative crystals, woods and composites are in the range  $0.05 < \lambda < 20$  and  $0 < \rho < 5$ . The definition (A2) pertains to plane stress, but is also valid for plane strain if  $s_{ij}$  is replaced by  $s'_{ij} = s_{ij} - s_{i3}s_{j3}/s_{33}$ .

The two-dimensional displacement field in anisotropic solids,  $u_i = u_i(x, y)$ ,  $i = 1, 2, 3$ , can be represented by three analytic functions  $f_1(z_1)$ ,  $f_2(z_2)$  and  $f_3(z_3)$ . The three complex variables,  $z_j = x + p_j y$  ( $\text{Im } p_j > 0$ ), are obtained by solving for  $p_j$  from an algebraic eigenvalue problem involving the elastic constants (e.g., Stroh, 1958; Lekhnitskii, 1981). The following results for orthotropic materials are extracted from Suo (1990).

When the principal orthotropy axes  $x_1$  and  $x_2$  coincide with  $x$  and  $y$ , the characteristic roots are

$$p_1, p_2 = \begin{cases} i\lambda^{-1/4}(n+m), & i\lambda^{-1/4}(n-m), & \text{for } 1 < \rho < \infty \\ \lambda^{-1/4}(in+m), & \lambda^{-1/4}(in-m), & \text{for } -1 < \rho < 1 \\ i\lambda^{-1/4}, & i\lambda^{-1/4} & \text{for } \rho = 1 \end{cases} \quad (\text{A3})$$

$$p_3 = i(s_{44}/s_{55})^{1/2}$$

where  $n = [(1+\rho)/2]^{1/2}$ ,  $m = |(1-\rho)/2|^{1/2}$ . The constant  $n$  appears in many formulae. The two fundamental matrices involved in the complex variable representation are

$$L = \begin{bmatrix} -p_1 & -p_2 & 0 \\ 1 & 1 & 0 \\ 0 & 0 & -1 \end{bmatrix}, \quad A = \begin{bmatrix} s_{11}p_1^2 + s_{12} & s_{11}p_2^2 + s_{12} & 0 \\ s_{21}p_1 + s_{22}/p_1 & s_{21}p_2 + s_{22}/p_2 & 0 \\ 0 & 0 & i\sqrt{s_{44}s_{55}} \end{bmatrix}. \quad (\text{A4})$$

The matrix  $B$  defined by  $B = iAL^{-1}$  takes the explicit form

$$B = \begin{bmatrix} 2n\lambda^{1/4}(s_{11}s_{22})^{1/2} & i((s_{11}s_{22})^{1/2} + s_{12}) & 0 \\ -i((s_{11}s_{22})^{1/2} + s_{12}) & 2n\lambda^{-1/4}(s_{11}s_{22})^{1/2} & 0 \\ 0 & 0 & (s_{44}s_{55})^{1/2} \end{bmatrix}. \quad (\text{A5})$$

Stroh (1958) showed that  $B$  is a positive definite Hermitian matrix for materials of general anisotropy. This can be verified directly from (A5) for our special case.

When the principal axes ( $x_1, x_2$ ) do not coincide with ( $x, y$ ) the above matrices can be obtained by an in-plane coordinate rotation:



$$R = \begin{bmatrix} \cos \theta & \sin \theta & 0 \\ -\sin \theta & \cos \theta & 0 \\ 0 & 0 & 1 \end{bmatrix} \quad (\text{A6})$$

where  $\theta$  is the angle from  $x_1$  to  $x$  and is positive in a counterclockwise sense. Ting (1982) showed that the characteristic roots in  $(x, y)$  coordinates are

$$p_j^* = (p_j \cos \theta - \sin \theta) / (p_j \sin \theta + \cos \theta) \quad (\text{A7})$$

and each column of  $A$  and  $L$  transforms like a *vector*:

$$A^* = RA, \quad L^* = RL. \quad (\text{A8})$$

It is obvious from its definition,  $B = iAL^{-1}$ , that the matrix  $B$  transforms like a second order tensor, i.e.

$$B^* = RBR^T. \quad (\text{A9})$$

The subsequent discussion involves quantities in the  $(x, y)$  coordinate (the starred quantities). For convenience the  $(*)$  is dropped hereafter, for example,  $z_j = x + p_j y$ . Once the potentials  $f_1(z_1)$ ,  $f_2(z_2)$  and  $f_3(z_3)$  are found for a boundary value problem, the displacements  $u_i$ , stresses  $\sigma_{ij}$ , and resultant forces  $T_i$  on an arc can be computed from

$$\begin{aligned} u_i &= 2 \operatorname{Re} \sum_{j=1}^3 A_{ij} f_j(z_j), & T_i &= -2 \operatorname{Re} \sum_{j=1}^3 L_{ij} f_j(z_j), \\ \sigma_{2i} &= 2 \operatorname{Re} \sum_{j=1}^3 L_{ij} f_j'(z_j), & \sigma_{1i} &= -2 \operatorname{Re} \sum_{j=1}^3 L_{ij} p_j f_j'(z_j). \end{aligned} \quad (\text{A10})$$

Here  $(\prime)$  is the derivative with respect to the argument. Notice from (A3) that the above representation breaks down when  $\rho = 1$ . A special representation for this degenerate case is given in Suo (1990). The matrix  $B$  with respect to the  $x, y$  axes, at an angle  $\theta$  from the principal axes, is

$$\begin{aligned} B_{11} &= 2n(s_{11}s_{22})^{1/2}(\lambda^{1/4} \cos^2 \theta + \lambda^{-1/4} \sin^2 \theta) \\ B_{22} &= 2n(s_{11}s_{22})^{1/2}(\lambda^{-1/4} \cos^2 \theta + \lambda^{1/4} \sin^2 \theta) \\ B_{12} &= \bar{B}_{21} = -n(s_{11}s_{22})^{1/2}(\lambda^{1/4} - \lambda^{-1/4}) \sin 2\theta + i((s_{11}s_{22})^{1/2} + s_{12}) \\ B_{33} &= (s_{44}s_{55})^{1/2}, \quad B_{13} = B_{23} = B_{31} = B_{32} = 0. \end{aligned} \quad (\text{A11})$$

This is obtained by the tensor rule (A9). Although the discussion is directed to orthotropic materials, the representation in (A10) is valid for general anisotropic materials, but the characteristic roots  $p_j$  and the three matrices  $A$ ,  $L$  and  $B$  should be computed according to the procedure outlined in Stroh (1958).

The results up to this point pertain to a single homogeneous material. The bimaterial matrix  $H$  of central importance is defined by

$$H \equiv B_1 + \bar{B}_2 \quad (\text{A12})$$

where the subscripts 1 and 2 indicate the two materials and the overbar denotes complex conjugation.  $H$  is obviously a positive definite Hermitian matrix. The explicit form of  $H$  for misoriented orthotropic bimaterials can be obtained from (A11), and several special cases are listed in the text.

## APPENDIX B: DISLOCATION INTERACTING WITH A TRACTION-FREE INTERFACE CRACK

Attention here is restricted to solids with  $(x, y)$  as a mirror plane and the in-plane deformation is considered. Only upper-left 2 by 2 matrices of  $L$ ,  $A$ ,  $B$  and  $H$ , and two potentials  $f_1(z_1)$  and  $f_2(z_2)$  are involved. Following Suo (1990), introduce a vector potential

$$\mathbf{f}(z) = \{f_1(z), f_2(z)\}. \quad (\text{B1})$$

Note the arguments of both  $f_1$  and  $f_2$  in (B1) are *identical*, and have the form  $z = x + \zeta y$  ( $\operatorname{Im} \zeta > 0$ ). Once a solution of  $\mathbf{f}(z)$  is obtained,  $f_1$  and  $f_2$  should be used with the arguments  $z_1$  and  $z_2$ , respectively, to compute the displacements and stresses from (A10). This strategy allows the standard matrix algebra to be used in conjunction with a number of analytic function concepts.

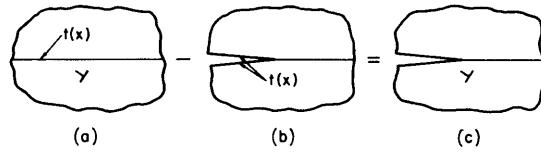


Fig. B1. A superposition scheme to obtain the kernel functions. (a) A dislocation embedded in a perfectly bonded bimaterial. (b) An interface crack with tractions prescribed on the faces, with no dislocation. (c) Interaction between a dislocation and a traction-free crack.

Consider a line dislocation perpendicular to the  $(x, y)$  plane with Burgers vector  $\mathbf{b} = \{b_x, b_y\}$  at the point  $(x_0, y_0)$  interacting with a traction free crack (Fig. B1c). The solution may be obtained by superposition of the following two problems: (a) a dislocation in a bimaterial with no crack (Fig. B1a); (b) an interface crack with traction prescribed to cancel the interface traction, but without dislocation (Fig. B1b). The solution procedure was outlined in Suo (1990) but only the case  $\varepsilon = 0$  was solved. Detailed below is the solution for the general case when  $\varepsilon \neq 0$ .

The solution to a dislocation in an infinite space of material 2 is (Eshelby *et al.*, 1953)

$$\mathbf{f}_0(z) = \{q_1 \ln(z-s_1), q_2 \ln(z-s_2)\}, \quad s_x = x_0 + p_x y_0, \quad \{q_1, q_2\} = (2\pi)^{-1} L_2^{-1} (B_2 + \bar{B}_2)^{-1} \mathbf{b}. \quad (\text{B2})$$

Constructed from  $\mathbf{f}_0(z)$ , the solution to problem (a) in Fig. B1 is

$$\mathbf{f}(z) = \begin{cases} L_1^{-1} H^{-1} (\bar{B}_2 + B_2) L_2 \mathbf{f}_0(z), & \text{in material 1} \\ \mathbf{f}_1(z) + L_2^{-1} \bar{H}^{-1} (\bar{B}_2 - \bar{B}_1) L_2 \bar{\mathbf{f}}_0(z), & \text{in material 2.} \end{cases} \quad (\text{B3})$$

The interface traction calculated from (B3) and (A10) is therefore

$$\mathbf{t}(x) = C \mathbf{f}'_0(x) + \bar{C} \bar{\mathbf{f}}'_0(x), \quad C = H^{-1} (B_2 + \bar{B}_2) L_2. \quad (\text{B4})$$

This traction is removed from the prospective crack faces using problem (b) in Fig. B1. The solution to the latter can be represented as

$$\mathbf{f}'(z) = \begin{cases} L_1^{-1} \mathbf{h}(z), & \text{in material 1} \\ L_2^{-1} H^{-1} H \mathbf{h}(z), & \text{in material 2.} \end{cases} \quad (\text{B5})$$

An eigenvector decomposition is employed to solve for  $\mathbf{h}$ :

$$\mathbf{h}(z) = h_1(z) \mathbf{w} + h_2(z) \bar{\mathbf{w}} \quad (\text{B6})$$

where  $\mathbf{w}$  is the eigenvector defined in the body of the text. The components are:

$$\begin{aligned} h_1(z) &= \frac{\chi_1(z)}{2\pi i} \int_{-\infty}^0 \frac{t(x) dx}{\chi_1^+(x)(x-z)}, \quad \chi_1(z) = z^{-1/2+ie}; \\ h_2(z) &= \frac{\chi_2(z)}{2\pi i} \int_{-\infty}^0 \frac{\bar{t}(x) dx}{\chi_2^+(x)(x-z)}, \quad \chi_2(z) = z^{-1/2+ie}. \end{aligned} \quad (\text{B7})$$

Here  $t$  is the component of  $\mathbf{t}$  in the sense  $\mathbf{t} = t\mathbf{w} + \bar{t}\bar{\mathbf{w}}$ , so that

$$\begin{aligned} t(x) &\equiv \frac{\bar{\mathbf{w}}^T H \mathbf{t}(x)}{\bar{\mathbf{w}}^T H \mathbf{w}} = \mathbf{c}_1^T \mathbf{f}'_0(x) + \mathbf{c}_2^T \bar{\mathbf{f}}'_0(x) \\ \mathbf{c}_1^T &= \frac{\bar{\mathbf{w}}^T (B_2 + \bar{B}_2) L_2}{\bar{\mathbf{w}}^T H \mathbf{w}}, \quad \mathbf{c}_2^T = e^{-2\pi e} \frac{\bar{\mathbf{w}}^T (B_2 + \bar{B}_2) \bar{L}_2}{\bar{\mathbf{w}}^T h \mathbf{w}}. \end{aligned} \quad (\text{B8})$$

Integration of (B7) gives

$$\begin{aligned} h_1(z) &= \frac{\mathbf{c}_1^T}{1 + e^{-2\pi e}} \begin{bmatrix} \left(1 - \frac{\chi_1(z)}{\chi_1(s_1)}\right) \frac{q_1}{z-s_1} \\ \left(1 - \frac{\chi_1(z)}{\chi_1(s_2)}\right) \frac{q_2}{z-s_2} \end{bmatrix} + \frac{\mathbf{c}_2^T}{1 + e^{-2\pi e}} \begin{bmatrix} \left(1 - \frac{\chi_1(z)}{\chi_1(\bar{s}_1)}\right) \frac{\bar{q}_1}{z-\bar{s}_1} \\ \left(1 - \frac{\chi_1(z)}{\chi_1(\bar{s}_2)}\right) \frac{\bar{q}_2}{z-\bar{s}_2} \end{bmatrix} \\ h_2(z) &= \frac{\bar{\mathbf{c}}_1^T}{1 + e^{2\pi e}} \begin{bmatrix} \left(1 - \frac{\chi_2(z)}{\chi_2(\bar{s}_1)}\right) \frac{\bar{q}_1}{z-\bar{s}_1} \\ \left(1 - \frac{\chi_2(z)}{\chi_2(\bar{s}_2)}\right) \frac{\bar{q}_2}{z-\bar{s}_2} \end{bmatrix} + \frac{\bar{\mathbf{c}}_2^T}{1 + e^{2\pi e}} \begin{bmatrix} \left(1 - \frac{\chi_2(z)}{\chi_2(s_1)}\right) \frac{q_1}{z-s_1} \\ \left(1 - \frac{\chi_2(z)}{\chi_2(s_2)}\right) \frac{q_2}{z-s_2} \end{bmatrix}. \end{aligned} \quad (\text{B9})$$